Proceedings of 12th Cambridge Workshop on Cool Stars, Stellar Systems, & The Sun, 2003 University of Colorado.

Detection of Differential Rotation in ψ Cap with Profile Analysis

A. Reiners[1], J.H.M.M. Schmitt[1], M. Kürster[2]

Abstract.
Differential rotation has been detected on the fast rotator ψ Cap (F5 V) using line profile analysis. The Fourier transforms of both Fe I $\lambda5775$ and Si I $\lambda5772$ are used to obtain a projected rotational velocity of $v\,\sin i = 42 \pm 1\,\mathrm{km\,s^{-1}}$. Modelling of the Fourier transformed profiles shows that the combined effects of equatorial velocity, inclination and differential rotation dominate the line profile while limb darkening and turbulence velocities have only minor effects. Rigid rotation is shown to be inconsistent with the measured profiles. Modelling the line profiles analogous to solar differential rotation we find a differential rotation parameter of $\alpha = 0.15 \pm 0.1$ comparable to the solar case. To our knowledge this is the first successful measurement of differential rotation through line profile analysis. A check with an observable directly obtained from the Fourier transform shows the internal consistency of our results.

1. Introduction

According to the standard paradigm of stellar activity differential rotation is a central ingredient for the magnetic dynamo presumed to underlie all activity phenomena. In a turbulent convection zone differential rotation is expected to be a central element of stellar activity. The interaction of rotation and convection naturally produces deviations from rigid rotation. One example for this effect is the Sun, whose equator rotates $\sim$20% faster than higher latitudes (Lang 1992). Direct predictions of the dependence of differential rotation on rotational velocity and spectral type have been made (e.g. Belvedere et al. 1980, Kitchatinov & Rüdiger 1999). Observations suggest a strong correlation between rotation and activity in late-type stars with many pieces of evidence summarized as "rotation-activity connection" (e.g. Hempelmann et al. 1995, Messina et al. 2001).

However, measurements of differential rotation among stars are either complicated or time-consuming or both. Three methods for determining stellar differential rotation have been used. (1) Variation of rotational periods; in the solar case spots emerge at certain latitudes and migrate across the surface from pole to equator. If the spots cause flux variations the rotational period of the

[1]Hamburger Sternwarte, Universität Hamburg, Gojenbergsweg 112, D-21029 Hamburg, Germany

[2]European Southern Observatory, Casilla 19001, Vitacura, Santiago 19, Chile

spot's latitude can be measured photometrically. In case of differential rotation the periods are expected to change with time (e.g. Donahue et al. 1996, Messina et al. 1999, Messina & Guinan 2001). (2) Doppler Imaging; On a solar like differentially rotating star spot groups migrating over the stellar surface disperse when the spots nearer to the equator move faster than those nearer to the pole. Two surface images of a star at two different times can reveal spot migrations and dispersions (e.g. Barnes et al. 2000, Donati & Collier Cameron 1997, Weber & Strassmeier 2001). For both methods (1) and (2) a huge amount of telescope time is needed what makes the observations of a larger sample very difficult. For the third method only one single line profile is sufficient: (3) Line profile analysis; direct examination of the subtle differences which exist between the line profile of a rigidly rotating star and that of a differentially rotating star. Although significant differences between the two cases are predicted, all previous attempts to measure differential rotation through line profiles alone remained unsuccessful and yielded results consistent with rigid rotation (Gray 1982, Dravins et al. 1990, Groot et al. 1996). At any rate, for a successful measurement one needs high spectral resolution and high signal to noise. With the Very Long Camera (VLC) of the Coudé Echelle Spectrograph (CES) at ESO's 3.6m telescope an instrumental setup satisfying these requirements is available. We report the detection of differential rotation in the F5 dwarf ψ Cap, to our knowledge the first successful measurement of differential rotation through line profiles.

2. Data

ψ Cap (HD 197 692, F5 V, $V_{\rm mag} = 4.13$, $v \sin i = 40\,{\rm km\,s^{-1}}$; Uesugi & Fukuda 1982) is the fastest rotator in a set of solar-like stars in the solar neighbourhood we observed on October 13, 2000 at ESO's 3.6m telescope (La Silla). The spectral resolution achieved with the CES / VLC setup was $R = 235\,000$ ($\sim 1.28\,{\rm km\,s^{-1}}$). Three consecutive exposures of ψ Cap of 270 s each covering the wavelength range between 5770 – 5810 Å were taken. The signal to noise ratio of the extracted spectrum is $S/N \sim 800$ per pixel with proper flat fielding and removal of interference pattern (Kürster 2001).

We concentrate our analysis on Fourier transforms of well isolated lines (Fe I λ5775 and Si I λ5772), for which continuum placement because of line blending is not a problem even for large $v \sin i$ values. The signal to noise ratio of our data is high enough to show the crucial features in the Fourier transform already from a single line.

Still, in Fe I λ5775 a small blend occurs from a neighbouring set of weak lines ~ 0.8 Å apart, the influence of which on differential rotation determination is not clear. During our observing run a spectrum of the slow rotator ι Psc (HD 222 368; F7 V) was taken. In Fig.1a both spectra are shown, with the profile of ι Psc shifted according to its relative radial velocity. Deblending of Fe I λ5775 was accomplished by, first, removing the line in the spectrum of ι Psc "by hand", broadening this template with $v_{\rm rot} = 40\,{\rm km\,s^{-1}}$ and subtracting it from the ψ Cap spectrum. In Fig. 1b the recorded spectrum as well as the modified spectrum of ψ Cap (blue) are shown. Obviously, the Si Iλ5772 equivalent widths of ψ Cap and ι Psc are the same, since it has been successfully removed (cf.

Fig.1b). The Fe I $\lambda 5775$ line appears symmetric, thus we think that deblending was successful.

3. Method of Analysis

Absorption line profiles are influenced by a number of different effects. An absorption line profile at any point on the star is determined by temperature, gravity, element abundances and atomic parameters. This "intrinsic" profile is Doppler broadened by velocity fields. Many efforts have been undertaken to distinguish these velocity fields, one of them being the stellar rotation (see Gray 1988 and references therein). In addition to the projected rotational velocity of the star, radial-tangential macro- and isotropic microturbulence (denoted with $\zeta_{\rm RT}$ and ξ resp.) turned out to be a reasonable parameterization of stellar atmospheric velocity fields. These parameterizations assume that Doppler broadenings can be treated as convolutions; and that the "intrinsic" profiles are identical over the apparent stellar disk. For fast rotators ($v\,\sin i\,>\,30\,\mathrm{km\,s^{-1}}$) and stationary atmospheres rotational broadening dominates and no complications occur with this assumption.

Interpreting the observed data profile $D(\lambda)$ as a a multiple convolution (denoted by $*$) between the intrinsic profile $F(\lambda)$ (including microturbulence broadening), the rotational broadening profile $G(\lambda)$, the instrumental profile $I(\lambda)$ and the macroturbulence profile $M(\lambda)$, $D(\lambda)$ can be written as

$$D(\lambda) = F(\lambda) * G(\lambda) * I(\lambda) * M(\lambda). \tag{1}$$

We calculated $F(\lambda)$ using the packages ATLAS9 (Kurucz 1979, Kurucz 1993) and BHT (Baschek et al. 1966). Atomic damping coefficients obtained from VALD (Kupka et al. 1999, Kurucz 1994) were included in the profile calculations; we chose solar metallicity and for the velocity dispersion of the opacity distribution function in ATLAS9 we used $1.0\,\mathrm{km\,s^{-1}}$. The temperature has been set to $T_{\rm eff}\,=\,6500\,\mathrm{K}$ (Blackwell & Lynas-Gray 1998). To calculate $G(\lambda)$ a modified version of a package developed and described by Townsend (1997) is used. The surface integration is carried out over about 25 500 visible surface elements. The adopted limb-darkening law is given by

$$I(\cos\theta)\;=\;I_0\,(1-\epsilon+\epsilon\cos\theta), \tag{2}$$

with θ denoting the angle between the surface element normal and the observer's line of sight and ϵ the limb darkening coefficient. We parametrize the differential rotation law through

$$\omega(l)\;=\;\omega_0-\omega_1\sin^2 l \tag{3}$$

with l being the latitude. Specifically, differential rotation is expressed in terms of $\alpha\,=\,\omega_1/\omega_0$. The differential rotation law (Eq. 3) is adopted from the solar case, where $\alpha_\odot\;=\;0.20$; a more general approach would expand $\omega(l)$ in terms of orthogonal polynomials. The instrumental profile $I(\lambda)$ has been determined from the shapes of calibration lamp lines, a correction for thermal broadening according to the lamp temperature of 120°C was applied. The macroturbulence broadening function $M(\lambda)$ is adopted from Gray (1992).

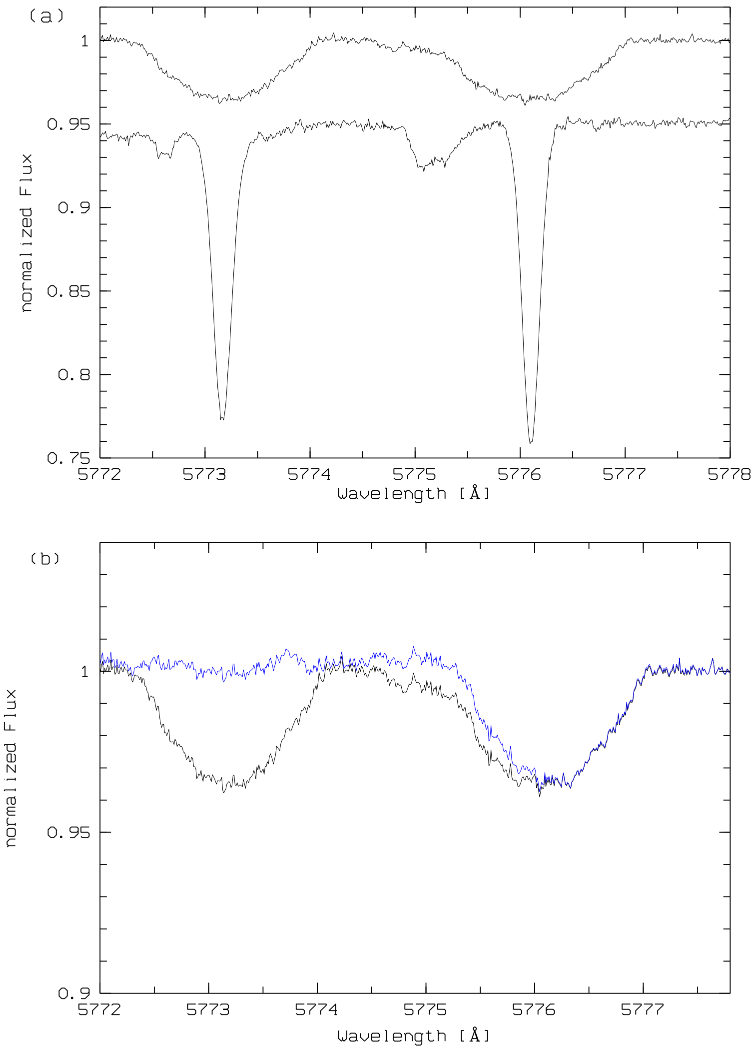

Figure 1. (a) Fe I $\lambda 5775$ (right) and Si I $\lambda 5772$ (left) lines of ψ Cap (upper line) and ι Psc (lower line; shifted along y-axis). (b) Original (black) and modified (blue) line profiles of ψ Cap (see text).

The contributions of different velocity fields are difficult to separate especially in the wavelength domain. In the Fourier domain convolutions become multiplications which are much easier to handle; the advantages of Fourier domain are discussed in detail by Gray (1992). In the Fourier domain Eq. 1 becomes

$$d(\sigma) = f(\sigma) \cdot g(\sigma) \cdot i(\sigma) \cdot m(\sigma). \tag{4}$$

The Fourier frequency σ is expressed in cycles / (km s^{-1}) = s km^{-1}. Especially zero positions of $g(\sigma)$ are not affected by multiplications with the functions $f(\sigma), i(\sigma)$ and $m(\sigma)$; $d(\sigma)$ shows the same zero positions as $g(\sigma)$.

Noise in Fourier domain can be expressed as $S_\sigma = S_\lambda \, \Delta\lambda \, N^{\frac{1}{2}}$ (Gray 1992), with S_λ being data noise and $\Delta\lambda$ step size in the wavelength domain, N is the number of data points. The Fourier transform of a real, symmetric profile yields a real function in the Fourier domain. Investigations of imaginary transforms of asymmetric lines show that these are no reliable tracers of profile properties (Gray 1980). We created a symmetric profile by mirroring the absorption profile at it's center; the achieved Fourier transform turned out to be stable against small variations of the center position. Rotational broadening, which dominates the line broadening in the case of ψ Cap, yields symmetric profiles. Asymmetries due to convection are believed to be of the order $v < 1\,\mathrm{km\,s^{-1}}$. In Fourier space this is $\sigma > 1\,\mathrm{s\,km^{-1}}$ while our analysis focuses on $\sigma < 0.04\,\mathrm{s\,km^{-1}}$. In the case of Fe I λ5775 an asymmetry may occur due to imperfect deblending, for Si I λ5772 no mechanism should contribute asymmetries of this order.

The Fourier transformed observed line profile was compared with a Fourier transformed model profile via a χ^2 test. Within our adopted modelling approach the following six fit parameters determine the model profiles: rotational velocity (v), inclination angle (i), differential rotation (α), limb darkening (ϵ), macro- (ζ_{RT}) and microturbulence (ξ). The χ^2-calculations have always been carried out directly on $d(\sigma)$. No further corrections have been applied to the data to avoid complications with amplified noise. Bruning (1984) pointed out that the convolution method induces systematic errors due to incorrectly estimated line depths especially in slow rotators. Our study is not focused on reproducing equivalent widths, which can be tuned e.g. by element abundances. The main goal is to reproduce the line shapes. Although we do not examine slow rotators in this study, normalized transformed profiles were used, that is, Fourier transformed profiles have been scaled to unity at $\sigma = 0$.

4. Results and Discussion

After a rough determination of $v \sin i$ a grid calculation in the six fit parameters was carried out. As to our model parameterization we note that this description contains parameters whose physics is poorly understood, i.e., the micro- and macroturbulence. We thus use χ^2 only as a relative parameter and not as an absolute criterion as to whether a model is acceptable or not; χ^2_n denotes the goodness of fit relative to the best fit, for which $\chi^2_\mathrm{n} = 1$ is set. For the actual grid we chose the parameter ranges of ϵ (0.4 – 0.8), ζ_RT (4.0 – 7.0) km s^{-1} and ξ (1.0 – 2.5) km s^{-1}. The rotation velocity was limited to $v < 120\,\mathrm{km\,s^{-1}}$ ($i > 20°$).

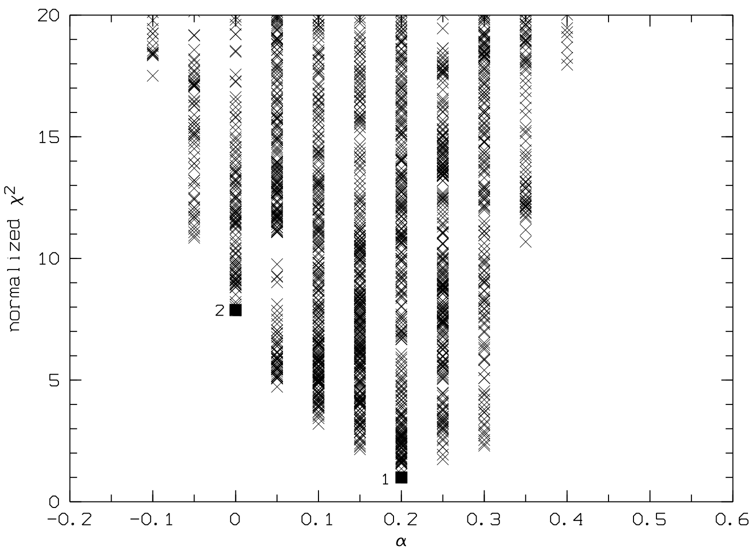

Figure 2. Normalized χ^2 vs. α for calculated models with various values of $v, i, \epsilon, \zeta_{\mathrm{RT}}$ and ξ (see text); each cross represents one set of parameters. Best fits of all models (1) and for rigid rotation (2) are denoted by full squares.

Goodness of fit calculations have been carried out independently on Fe I $\lambda5775$ and Si I $\lambda5772$; both lines show identical results. In the following we show only the results for Fe I $\lambda5775$.

In Fig. 2 we plot the resulting χ^2_{n} as a function of the differential rotation parameter α; for each fixed value of α, we plot the χ^2_{n} values obtained by varying all other model parameters. Clearly, a well defined lower envelope curve exists with a minimum at $\alpha = 0.20$. The best fits for differential rotation (here $\alpha = 0.20$; $\chi^2_{\mathrm{n}} = 1$, Model 1) and rigid rotation ($\alpha = 0.0$, $\chi^2_{\mathrm{n}} = 7.9$, Model 2) are marked by full squares; all parameters are shown in Tab. 1.

Table 1. Parameters of best fitting models for rigid and differential rotation

Model	v	i	α	ϵ	ζ_{RT}	ξ	χ^2_n
1	$43\frac{\mathrm{km}}{\mathrm{s}}$	80°	0.20	0.6	$4.0\frac{\mathrm{km}}{\mathrm{s}}$	$1.0\frac{\mathrm{km}}{\mathrm{s}}$	1.0
2	$48\frac{\mathrm{km}}{\mathrm{s}}$	60°	0.00	0.8	$7.0\frac{\mathrm{km}}{\mathrm{s}}$	$2.5\frac{\mathrm{km}}{\mathrm{s}}$	7.9

In Fig. 3 we plot the corresponding profiles in the Fourier domain; obviously, Model 1 provides a much better fit than Model 2, which is not an adequate description of our data. While no statistical uncertainties can be given on our χ^2_{n}-values, Fig. 3 shows χ^2_{n}-values of 7.9 to be clearly unacceptable.

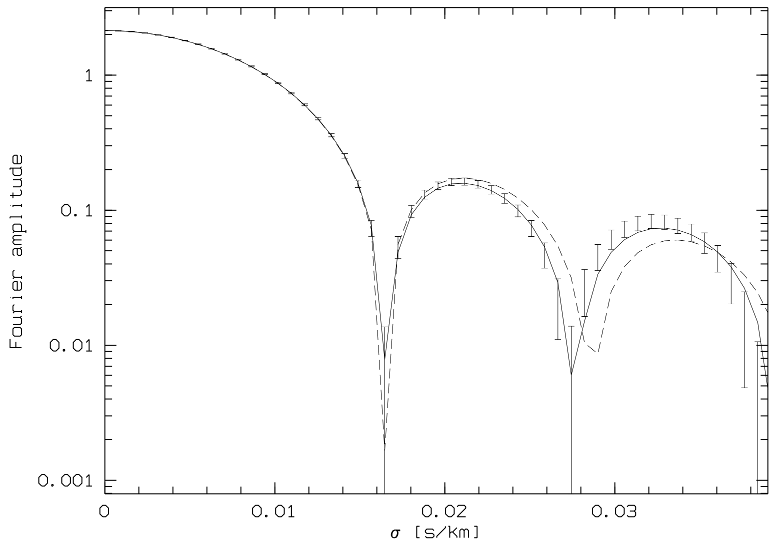

Figure 3. The Fourier transformed data indicated by error bars. Best fits for differential rotation (α = 0.20; full line, Model 1) and rigid rotation (α = 0.0; dashed line, Model 2) are shown. See Tab. 1 for parameters.

Inspection of the calculated $\chi^2_{\rm n}$-grid shows that the parameters $\epsilon, \zeta_{\rm RT}$ and ξ produce only second order effects; the fits are driven by the chosen values of v, i and α, and we cannot determine all model parameters independently. Therefore, we fixed the values $\epsilon = 0.6$ (Carbon & Gingerich 1969), $\zeta_{\rm RT} = 6.0\,{\rm km\,s^{-1}}$ and $\xi = 1.0\,{\rm km\,s^{-1}}$ (Gray 1988 and references therein). We emphasize that our subsequent findings do not require these specific parameter settings, and that the influences of ϵ, $\zeta_{\rm RT}$ and ξ are too small to revoke the effects of α, v and i. For the given parameters the best fit value for $v\,\sin i$ is $42.3\,{\rm km\,s^{-1}}$. We estimate the total systematic errors to be $\approx 1\,{\rm km\,s^{-1}}$. Models outside the range $42.3 \pm 1\,{\rm km\,s^{-1}}$ all have $\chi^2_{\rm n} > 5$.

Theoretical investigations of the line profile behaviour in Fourier space show that with differential rotation $\alpha \neq 0$ the inclination i becomes important (e.g. Bruning 1981). For comparable values of $v\,\sin i$ the best fit values of α and i are correlated. In Fig. 4 we consider calculated models with fixed ϵ, $\zeta_{\rm RT}$ and ξ, $v\,\sin i$ between 41.3 and $43.3\,{\rm km\,s^{-1}}$ and varying α, v and i. Three groups of models are distinguished; $\chi^2_{\rm n} < 5\,(\bullet)$, $5 < \chi^2_{\rm n} < 10\,(\circ)$ and $\chi^2_{\rm n} > 10\,(\cdot)$.

A well defined area of reliable fits in the $\alpha - i$ plot emerges. All fits with $\chi^2_{\rm n} < 10$ show $\alpha > 0.0$. Although we used no absolute criterion on wheter a model is acceptable, the estimation of systematic errors and a comparison with Fig. 3 shows that the threshold $\chi^2_{\rm n} < 10$ is rather conservative.

A variety of combinations of equatorial velocity and inclination seems possible for $\alpha > 0$. A smaller differential effect is preferred for faster rotating models. For extremely high values of $v > 200\,{\rm km\,s^{-1}}$ rigid rotation might be argued, but such velocities seem unlikely given the age of ψ Cap of $\sim 2\,10^9$ a

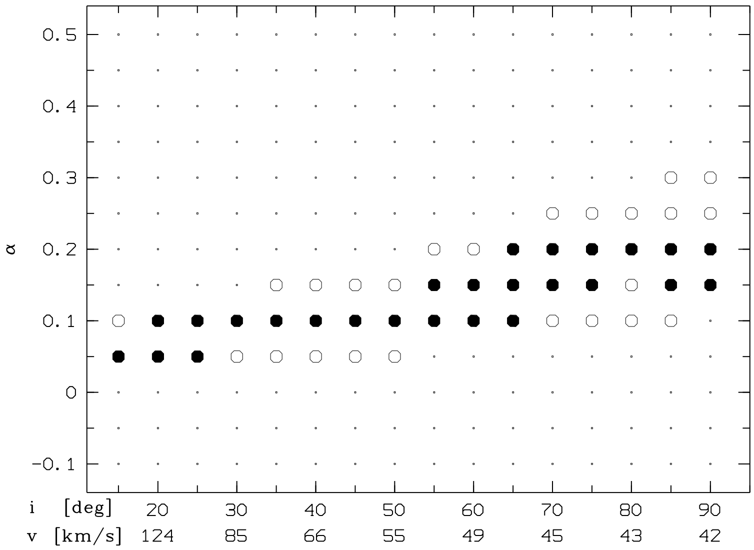

Figure 4. χ^2_n of fits to Fe I $\lambda 5775$ with $41.3\,\mathrm{km\,s^{-1}} < v \sin i < 43.3\,\mathrm{km\,s^{-1}}$, $\epsilon = 0.6$, $\zeta_\mathrm{RT} = 6.0\,\mathrm{km\,s^{-1}}$ and $\xi = 1.0\,\mathrm{km\,s^{-1}}$ in the $\alpha - i$ (v) plane: $\chi^2_\mathrm{n} < 5\,(\bullet)$; $5 < \chi^2_\mathrm{n} < 10\,(\circ)$; $\chi^2_\mathrm{n} > 10\,(\cdot)$.

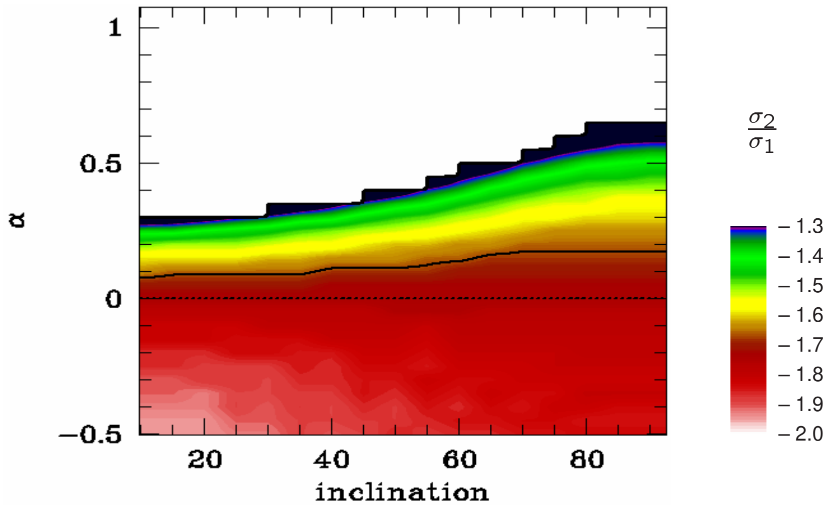

Figure 5. Ratio σ_2/σ_1 of second (σ_2) and first (σ_1) zeros of a Fourier transformed line profile in the $\alpha - i$ plane ($\epsilon = 0.6$). From a measured value of σ_2/σ_1 an associated region can be found in the $\alpha - i$ plane. For ψ Cap we found $\sigma_2/\sigma_1 = 1.65 \pm 0.01$ which is marked with the solid line. As can be seen, σ_2/σ_1 is a well suited obeservable to determine solar-like differential rotation ($\alpha > 0$) but is not adequate for detection of anti-solar differential rotation ($\alpha < 0$).

(Lachaume et al. 1999). Even the minimum rotational velocity of $42\,\mathrm{km\,s^{-1}}$ seems uncommonly high. From Fig. 4 we derive $\alpha = 0.15 \pm 0.1$. The identical result was found for Si I λ5772, where the same procedure was applied.

As a consistency check we also determined the amount of differential rotation directly by the zeros of $d(\sigma)$, which are inferred from the rotational broadening profile $g(\sigma)$ (cf. Fig. 3). The ratio of the second (σ_2) and the first (σ_1) zeros σ_2/σ_1 is sensitive to differential rotation as well as limb darkening (see e.g. Bruning 1981). For a rigid rotator σ_2/σ_1 is in the range 1.72 ... 1.83 depending on which value of ϵ is chosen (Dravins et al. 1990). From the Fourier transform of ψ Cap we derive $\sigma_2/\sigma_1 = 1.65 \pm 0.01$, which clearly is outside the range accessible by rigid rotation and variable limb darkening only. In Fig. 5 σ_2/σ_1 is shown colour-coded in an $\alpha - i$ grid for $\epsilon = 0.6$. With a given value of σ_2/σ_1 a range of possible combinations in the $\alpha - i$ plane can be achieved. The solid line shows the value measured for ψ Cap and marks exactly the same region found in Fig. 4 by detailed atmospheric modelling. Thus σ_2/σ_1 can be used as an easily measurable observable to search for differential rotation in fast rotators.

To summarize, differential rotation has been established for the rapid rotator ψ Cap independently from two absorption line profiles. While ψ Cap rotates at least 20 times faster than the Sun, its differential rotation is comparable to the solar value, but not with the differential rotation patterns determined from Doppler images of the fast rotators AB Dor (Donati & Collier Cameron 1997) and PZ Tel (Barnes et al. 2000). As direct predictions for a F5 dwarf have not been calculated by (Kitchatinov & Rüdiger 1999) and the rotation period of ψ Cap is only poorly determined, the consistency between our result and the model is not clear. Assuming $R = 1.2\,\mathrm{R}_\odot$ and $i = 90°$, we find for ψ Cap the rotation law $\omega(l) = 4.38 - 0.66 \sin^2 l\,\mathrm{rad/d}$; ψ Cap does not rotate like a rigid body as suggested for AB Dor and PZ Tel. To compare theory and observations more detailed predictions especially on spectral type dependence and a greater sample of direct observations are needed. In particular verification of the differential rotation results of line profile analysis and Doppler imaging for the same star will be instructive.

Acknowledgments. A.R. acknowledges financial support from Deutsche Forschungsgemeinschaft under DFG-SCHM 1032/10-1.

References

Barnes J.R., Collier Cameron A., James D.J., Donati J.-F. 2000, MNRAS, 314, 162

Baschek B., Holweger H., Traving G. 1966, Abhandl. Hamburger Sternwarte, 8, 26

Belvedere G., Casassus L., Stix M. 1980, A&A, 88, 240

Blackwell D.E., Lynas-Gray A.E. 1998, A&AS, 129, 505B

Bruning D.H 1981, ApJ, 248, 274

Bruning D.H 1984, ApJ, 281, 830

Carbon D.F., Gingerich O. 1969, in Theory and Observation of normal stellar atmospheres, MIT Press, Ed. Gingerich O.

Donahue R.A., Saar S.H., Baliunas S.L. 1996, ApJ, 466, 384

Donati J.-F., Collier Cameron A. 1997, MNRAS, 291, 1

Dravins D., Lindegren L., Torkelsson U. 1990, A&A, 237, 137

Gray D.F. 1980, ApJ, 235, 508

Gray D.F. 1982, ApJ, 258, 201

Gray D.F. 1988, Lectures on spectral-line analysis: F, G and K stars, The Publisher, Arva

Gray D.F. 1992, The observation and analysis of stellar photospheres, Cambridge Univ. Press, Cambridge

Groot P.J., Piters A.J.M., van Paradijs J. 1996, A&AS, 118, 545

Hempelmann A., Schmitt J.H.M.M., Schultz M., Rüdiger G., Stępien K. 1995, A&A, 294, 515

Kitchatinov L.L., Rüdiger G. 1999, A&A, 344, 911

Kürster M. 2001, The CES User Manual; http://www.ls.eso.org/lasilla/Telescopes/360cat/ces/

Kurucz R.L. 1979, ApJS, 40, 1

Kurucz R.L. 1993, in Peculiar versus normal phenomena in A-type and related stars, IAU Coll. 138, Eds. Dworetsky et al., ASP Conf. Series, 87

Kurucz R.L. 1994, SAO, Cambridge, CDROM 20-22

Kupka F., Piskunov N.E., Ryabchikova T.A., Stempels H.C., Weiss W.W. 1999, A&AS, 138, 119

Lachaume R., Dominik C., Lanz T., Habing H.J. 1999, A&A, 348, 897

Lang K.R. 1992, Astrophysical Data I. Planets and Stars. Springer-Verlag, Berlin

Messina S., Guinan E.F., Lanza A.F., Armbruster C. 1999, A&A, 347, 249

Messina S., Rodonò M., Guinan E.F. 2001, A&A, 366, 215

Messina S., Guinan E.F., CS 12, Poster 06.07

Townsend R. 1997, MNRAS, 284, 839

Uesugi, A., Fukuda, I., Catalogue of stellar rotational velocities (revised), Kyoto: University of Kyoto, Departement of Astronomy 1982, Rev.ed

Weber M., Strassmeier K.G. 2001, A&A, 373, 974